Dynamics of a *Volvox* Embryo Turning Itself Inside Out

Stephanie Höhn, Aurelia R. Honerkamp-Smith, Pierre A. Haas, Philipp Khuc Trong, and Raymond E. Goldstein
Department of Applied Mathematics and Theoretical Physics, Centre for Mathematical Sciences, University of Cambridge, Wilberforce Road, Cambridge CB3 0WA, United Kingdom
(Received 4 September 2014; published 27 April 2015)

Deformations of cell sheets are ubiquitous in early animal development, often arising from a complex and poorly understood interplay of cell shape changes, division, and migration. Here, we explore perhaps the simplest example of cell sheet folding: the "inversion" process of the algal genus *Volvox*, during which spherical embryos turn themselves inside out through a process hypothesized to arise from cell shape changes alone. We use light sheet microscopy to obtain the first three-dimensional visualizations of inversion *in vivo*, and develop the first theory of this process, in which cell shape changes appear as local variations of intrinsic curvature, contraction and stretching of an elastic shell. Our results support a scenario in which these active processes function in a defined spatiotemporal manner to enable inversion.

DOI: 10.1103/PhysRevLett.114.178101 PACS numbers: 87.17.Pq, 02.40.-k, 46.25.-y, 87.10.Pq

Lewis Wolpert's comment, "It is not birth, marriage, or death, but gastrulation which is truly the most important time in your life" [1], emphasizes the central role of cell sheet folding in developmental biology. Gastrulation is the process by which a convex mass of cells develops an invagination that leads to the formation of the gut, and eventual change of topology to that of a torus. Processes involving invagination pervade tissue formation and include ventral furrow formation in *Drosophila* [2] as well as neurulation [3] and optic cup formation in vertebrates [4]. One of the common themes accompanying the bending and stretching of cell sheets during invaginations is a set of cell shape changes, in particular transitions from columnar to wedge shapes [5]. However, cell sheet deformations in animal model organisms frequently also involve cell division, migration, and intercalation that obscure the specific role of shape changes. Thus, it has proven difficult to identify model systems amenable to a simple physical description.

By contrast, as we emphasize here, the green flagellated alga *Volvox* [6] provides an elegantly simple system to study the dynamic morphology of cell sheets. When cell division is complete, a *Volvox* embryo consists of several thousand cells forming an approximately spherical monolayer enclosed by a fluid-filled "embryonic vesicle" [6,7]. Each cell is linked to its neighbors by a network of cytoplasmic bridges (CB), thin membrane tubes resulting from incomplete cell division. Some cells at the anterior pole of the embryo are not connected, resulting in an opening called the phialopore [8,9]. At this stage, those cell poles whence emanate the flagella point into the sphere. This situation is corrected by a major morphological event, during which the cell sheet turns itself inside out. This "inversion" brings the flagella to the outside, enabling motility [10,11]. The duration of inversion in *Volvox* ranges from 45 to 80 minutes.

The sequence of deformations that *Volvox* embryos [Fig. 1(a)] undergo during inversion varies from species to species and is broadly divided into two types. In type-A inversion [10–12], four outward-curling lips open at the anterior pole of the embryo and peel back [Fig. 1(b)], while type-B inversion [12,13] starts with a circular invagination at the equator. Simultaneously, the posterior hemisphere moves into the anterior while gradually inverting. The phialopore then widens and stretches over the inverted posterior (Fig. 1(c) and Video 1 in the Supplemental Material [14]). Only type-B inversion shares the process of invagination with the aforementioned examples of cell sheet deformations in animals [13].

Previous studies of type-A inversion, including chemical treatments and the characterization of a mutant strain [9,10,15–17], pointed to waves of active cell shape changes combined with cell movements relative to the cytoplasmic bridges as the mechanism driving inversion. Similar cell shape changes and reorganization of cytoplasmic bridges have been reported for type-B inversion [13]. Inversion starts when cells around the phialopore of type-A embryos or at the equator of type-B embryos [Fig. 1(d)], respectively, become wedge shaped by developing narrow basal stalks. Simultaneously, these cells move relative to the cytoplasmic bridges until they are connected at the tips of their stalks [Fig. 1(e)] [13,17]. It is natural to view the splay induced by the combination of shape changes and bridge motion as inducing a local intrinsic curvature in the cell sheet, thus connecting inversion to the many areas in cellular biophysics, from vesicular budding [18] to structures in the endoplasmic reticulum [19], in which intrinsic curvature plays a role. In addition to wedge-shaped cells,

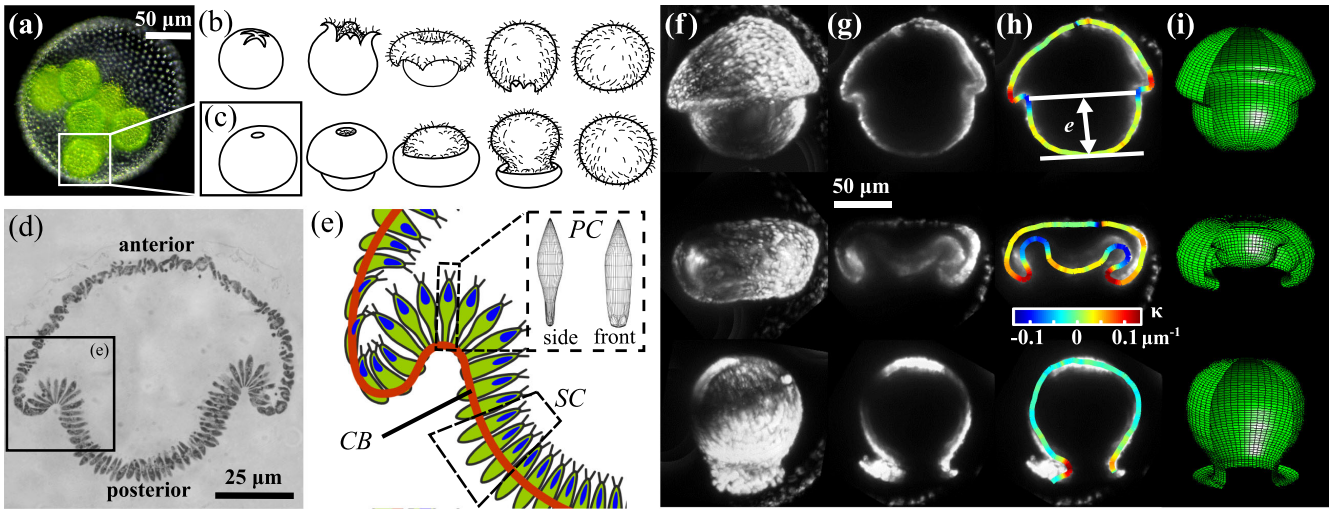

FIG. 1 (color online). Embryonic inversion in *Volvox*. (a) Adult *V. globator* spheroid containing multiple embryos. (b) Embryo undergoing type-A inversion (e.g., *V. carteri*). (c) Embryo undergoing type-B inversion (e.g., *V. globator*, *V. aureus*). (d) Light micrograph shows semi-thin section of *V. globator* embryo exhibiting different cell shapes. (e) Schematic representation of cells in region marked in (d). PC: paddle-shaped cells, two different views illustrate anisotropic shape; SC: spindle-shaped cells; red line: position of cytoplasmic bridges (CB). (f) 3D renderings of a single *V. globator* embryo in three successive stages of inversion. (g) Optical midsagittal cross sections of embryo in (f). (h) Traced cell sheet contours overlaid on sections in (g), with color-coded curvature κ. (i) Surfaces of revolution computed from averaged contours. Panels (d) and (e) modified from [13].

other cell shape changes specific to type-B inversion occur in the anterior and posterior hemispheres [13]. Their role in inversion and the interplay between active deformations and passive responses of the cell sheet have remained ambiguous due to the lack of dynamic quantification.

The majority of previous work on inversion used electron microscopy to acquire static high-resolution snapshots of embryos arrested at a particular stage of inversion. A single study [15] sought to analyze the dynamics of type-A inversion using light microscopy. Here, using embryos of *V. globator*, we report the first three-dimensional time-lapse visualizations of type-B inversion dynamics, and we develop the first mathematical descriptions of specific stages of this process.

A selective plane illumination microscope was assembled as previously described [20], with modifications to accommodate an alternate laser (473 nm, 144 mW, Extreme Lasers, Houston, TX) and camera (CoolSNAP MYO, 1940×1460 pixels; Photometrics, AZ, USA). Autofluorescence ($\lambda > 500$ nm) of the algae was used for imaging. Wild-type strain *V. globator* Linné (SAG 199.80) was obtained from the Culture Collection of Algae at the University of Göttingen, Germany [21], and cultured as previously described [22] with a cycle of 16 h light at 24 °C and 8 h dark at 22 °C. Image stacks of mother spheroids containing 5–9 embryos were recorded at intervals of 20–300 s over 2–4 hours to capture inversion of all embryos. Where necessary, data sets were resliced using AMIRA (FEI, OR, USA). The outline of the cell sheet was manually traced on midsagittal sections [Fig. 1(h)] using IMAGEJ [23]. We quantified inversions of 10 embryos with initial diameters of ~70–130 μm.

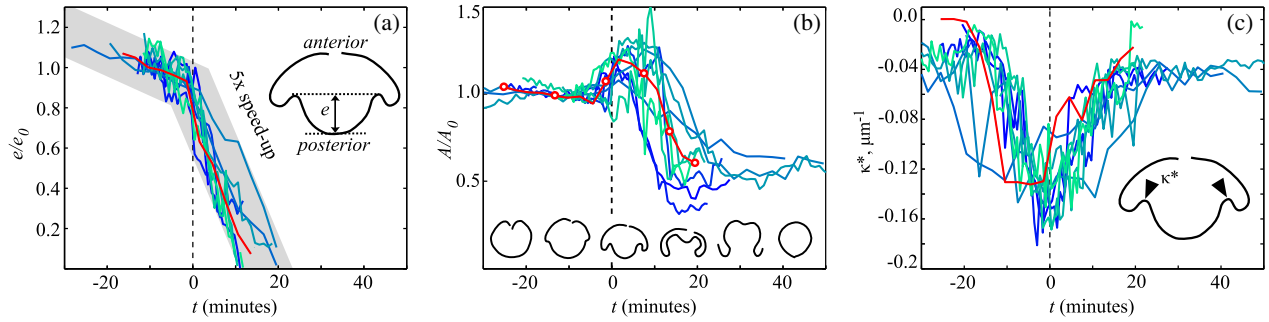

FIG. 2 (color online). Dynamic characterization of inversion in *V. globator*. Red lines in (a)–(c) are data for one representative embryo, whose traced outlines are shown in (b). (a) Distance e from posterior pole to bend region, normalized by its value e_0 at $t \approx -10$ min, decreases at a speed that increases abruptly midinversion. (b) Surface area A of the embryo, normalized by its value A_0 at $t \approx -20$ min, peaks after $t = 0$, and then decreases. Traced embryo shapes correspond to time points indicated by open circles on the red curve. (c) Most negative embryo curvature κ^* in the bend region peaks concurrently with speed-up.

We focus on three key quantities derived from the cross-sectional shapes. Shown in Fig. 2, these are the distance e from the posterior pole to the circular bend region [Fig. 1(h)], the embryonic surface area A, and the most negative value κ^* of the curvature in the bend region. A spline was fit to the traced line, and this curve yielded the signed curvature κ [Fig. 1(h)]. To compute the surface area of the embryo during inversion, we constructed a surface of revolution [Fig. 1(i)] from the average of the two halves of a midsagittal slice (see also Supplemental Material [14]). The distance e was separately measured for both embryo halves and then averaged.

At the beginning of inversion, embryos develop "mushroom" shapes [Figs. 1(f)–1(i)]. The distance e initially decreases at a constant speed $U = \dot{e}$ [Fig. 2(a)], but, similar to type-A inversion [15], the speed increases abruptly by a factor of ~5 midinversion, to reach values of $U \sim 0.03$ μm/s. The speed-up nearly coincides with the peak in the curvature κ^* in the bend region [Fig. 2(c)]. For the subsequent analysis of experimental results, we reference all times relative to this speed-up, defined as $t = 0$. Over tens of minutes prior to $t = 0$, there is evidence for a decrease in surface area (~10%), followed by a significant increase (20%–30%) at or shortly after $t = 0$, before a decrease to about 55% of its initial value [Fig. 2(b)]. The transient increase in surface area is consistent with previously reported flattened disk-shaped cells in the anterior hemisphere (Fig. 12C in [13]).

To provide a test of the idea that a localized region of intrinsic curvature can drive inversion, we consider the axisymmetric deformations of a thin elastic spherical shell of thickness h and undeformed radius R under quasistatic variations of its intrinsic curvature. A similar approach, phrased in terms of bending moments rather than preferred curvatures, was used previously to study the initiation of gastrulation in *Xenopus laevis*, likewise involving invagination of a spherical embryo [24].

As shown in Fig. 3, let s be arclength along the undeformed shell and $r_0(s)$ be the distance to the axis of revolution, and $S(s)$ and $r(s)$ be the corresponding quantities for the deformed shell. The meridional and circumferential stretches $f_s = dS/ds$, $f_\phi = r/r_0$ define the strains

$$E_s = f_s - f_s^0, \qquad E_\phi = f_\phi - f_\phi^0, \tag{1}$$

and curvature strains

$$K_s = f_s\kappa_s - f_s^0\kappa_s^0, \qquad K_\phi = f_\phi\kappa_\phi - f_\phi^0\kappa_\phi^0. \tag{2}$$

Here, κ_s and κ_ϕ are the meridional and circumferential curvatures of the deformed shell. As in the Helfrich model [25] for membranes and generalizations that include "area elasticity" [26], f_s^0, f_ϕ^0 and $\kappa_s^0, \kappa_\phi^0$ introduce preferred stretches and curvatures, respectively. Adopting a Hookean model [27] with elastic modulus E and Poisson ratio ν, the deformed shell minimizes the energy

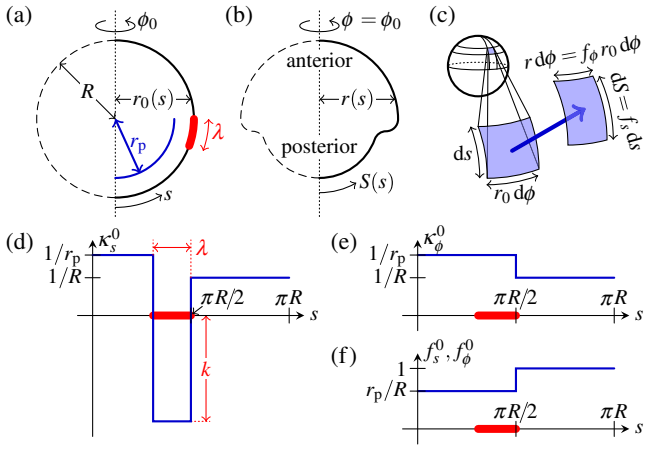

FIG. 3 (color online). Elastic model. (a) Undeformed elastic spherical shell of radius R and thickness h. (b) Deformed configuration of the shell. (c) Stretches f_s, f_ϕ relate undeformed and deformed geometries. (d) Imposed intrinsic curvature $\kappa_s^0 = -k < 0$ in a region of width λ just below the equator. Posterior contraction modifies the intrinsic properties (d,e,f) by introducing a posterior radius $r_p < R$.

$$\mathcal{E} = \frac{\pi Eh}{1-\nu^2}\int_0^{\pi R} r_0(E_s^2 + E_\phi^2 + 2\nu E_s E_\phi)ds + \frac{\pi Eh^3}{12(1-\nu^2)}\int_0^{\pi R} r_0(K_s^2 + K_\phi^2 + 2\nu K_s K_\phi)ds. \tag{3}$$

In computations, we take $\nu = 1/2$ and $\varepsilon \equiv h/R = 0.15$.

To test whether the initial invagination and the movement of the posterior are, indeed, results of local changes in the intrinsic curvature, we consider the formation of a region of width λ of preferred curvature $\kappa_s^0 = -k < 0$ [Fig. 3(d)]. Examination of thin sections [Fig. 1(d)] suggests an early value $\lambda \approx 0.1\pi R$ and $kR \approx 10$–20. Modifying κ_s^0 rather than κ_ϕ^0 accounts for the previously observed anisotropy of the wedge-shaped ("paddle-shaped") cells in the bend region [Fig. 1(e)] [13].

We find that solely imposing a preferred curvature leads to a "purse-string" effect [Fig. 4(a)] over large ranges of the parameters k and λ. Yet, *V. globator* embryos adopt a mushroom shape not captured by this description, suggesting that additional active cell shape changes are needed. Indeed, cells throughout the posterior hemisphere have been reported to adopt a thinned spindle shape at the start of inversion [13]. Interestingly, strains in the model decay rapidly away from the bend region [Fig. 4(d)], thus suggesting that other cell shape changes, both in the anterior and the posterior hemispheres, arise actively due to cell-intrinsic forces. To include active posterior contraction in our model, we define a reduced posterior radius $r_p < R$ and modify $f_s^0, f_\phi^0, \kappa_s^0, \kappa_\phi^0$ accordingly [Figs. 3(d), 3(e), and 3(f)]. For realistic parameter values, $r_p/R \approx 0.7$ and $kR \approx 20$ [13], the model now successfully yields mushroom shapes [Fig. 4(b)] that are in quantitative agreement with an average experimental shape [Figs. 4(f)

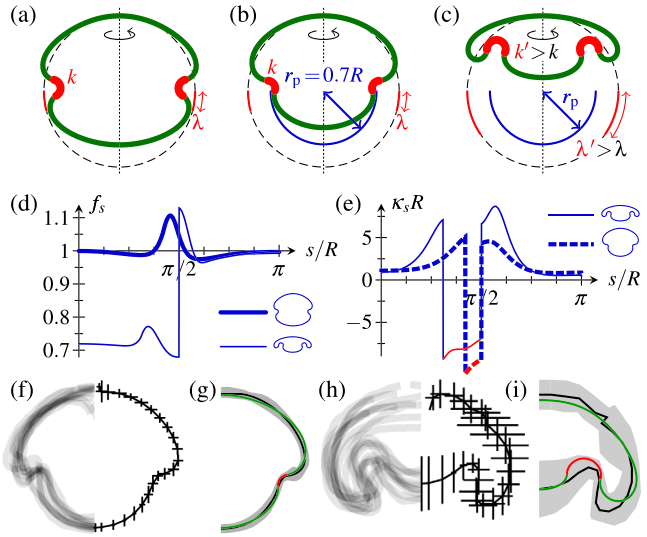

FIG. 4 (color online). Results of elastic model and comparison with experiment. (a) In the absence of contraction, there is a purse-string effect. (b) Correct "mushroom" shapes are obtained once contraction is included, which allows (c) the inverted posterior to fit into the anterior hemisphere. (d) Decay of strains in both hemispheres away from bend region. (e) Asymmetry of meridional curvatures of contracted shapes corresponds to passive formation of second bend region. (f), (h) Outlines (gray) of 10 embryos in an early stage ($e/e_0 = 0.97 \pm 0.07$) and a later stage ($e/e_0 = 0.49 \pm 0.09$) of inversion, and averages (black). Bars indicate standard deviations. (g), (i) Computed shapes (green) lie within a standard deviation (gray areas) of average shapes.

and 4(g)]. *In vivo*, more cells in the bend region become wedge shaped as invagination progresses. In the model, we capture this by enlarging k and λ, and find that, while an uncontracted posterior does not fit into the anterior hemisphere, a contracted posterior does fit [Fig. 4(c)]. This is similar to type-A inversion: embryos in which posterior contraction is prevented biochemically fail to complete inversion [16]. While matching the *in vivo* shapes qualitatively, this computed shape [Fig. 4(c)] is more flattened than in experiments [Fig. 4(h)]. A quantitative fit can, for example, be achieved by extending the model to allow anisotropic inhomogeneous stretching of the anterior (Fig. 4(i) and Supplemental Material [14]).

The question remains whether active anterior expansion, as suggested by (i) disk-shaped cells there, (ii) the increase in A, and (iii) the aforementioned rapid decay of passive strains, also contributes to mushroom shapes. Indeed, defining an increased anterior radius, instead of posterior contraction, also produces mushroom shapes (Fig. S2 of Supplemental Material [14]). The small (∼2.5%) decrease in surface area observed after formation of the bend region is substantially smaller than the ∼25% we estimate would occur if posterior contraction alone were present, so we infer that compensating anterior expansion has likely begun before $t = 0$. Expansion then eventually dominates contraction, leading to the observed increase in surface area [Fig. 2(b)]. *In vivo*, this expansion may facilitate the fit of the posterior into the anterior, a previously unrecognized role for active cell shape changes in the anterior.

In contrast to *V. globator*, *V. aureus* adopts "hourglass" shapes like that in Fig. 4(a) before progressing to mushroom shapes [28]. This suggests that the beginning of inversion in *V. aureus* is purely curvature-driven, with expansion and/or contraction only arising later. All of this suggests that, in type-B inversion, posterior contraction and anterior expansion act as complementary strategies to create a disparity between the anterior and posterior radii. The relative timing and position of the initial invagination, contraction, and expansion may differ between species.

In the present model, the meridional curvature [Fig. 4(e)] of shapes that reproduce late invagination [Figs. 4(c) and 1(h) middle] shows an asymmetry between the posterior and anterior hemispheres corresponding to the formation of a second bend region with increased positive curvature. In previous microscopic observations, this region has been termed the "anterior cap" [13]. In the elastic model, it arises as a passive material response to the negative intrinsic curvature imposed at the adjacent equatorial region. Note that, whereas open elastic filaments can easily adopt shapes in which the local curvature is everywhere equal to the intrinsic curvature [29], the situation for sheets is much more constrained, and the local intrinsic curvature cannot simply be inferred from the equilibrium shape. Imposing this positive curvature actively, instead of the negative intrinsic curvature, does not lead to correct embryo shapes irrespective of contraction (see Supplemental Material [14]). This supports our original assumption that active formation of wedge-shaped cells drives invagination.

The sudden increase in the speed of posterior inversion when κ^* peaks is reminiscent of a mechanical snap-through [30], as suggested in earlier work on type-A inversion [15], yet conventional snap-throughs of elastic materials do not proceed at constant speed. Here, we consider a possible explanation for the constant speed in the most parsimonious of settings, that of the snap-through of a Pogorelov dimple [31] of depth e on an elastic spherical shell of radius R and thickness h. A scaling argument [31], balancing bending and stretching at the dimple edge, shows that the elastic driving force of the snap-through scales as $Eh^{5/2}e^{1/2}/R$. The sources of dissipation in such a system are myriad. While we postpone a detailed discussion [32], we note that the hydrodynamic resistance associated with the velocity gradients at the dimple edge scales as $\mu U e^{1/2} R^{1/2}$ [32], where μ is the fluid viscosity. Hence, there is an e-independent snap-through speed $U \sim Eh^{5/2}/\mu R^{3/2}$. A more detailed analysis [32] shows that this scenario is also compatible with the kink observed in experiments. However, this argument cannot rule out other dissipation or cell-intrinsic mechanisms.

In summary, we have shown that a simple quasistatic model, combining changes in intrinsic curvature with active contraction and expansion, is consistent with embryo shapes during type-B inversion. We are led to hypothesize that bending, posterior contraction and some mechanism of

anterior stress relief are common features of inversion in the genus *Volvox* which allow embryos to overcome geometric constraints during inversion. Whether the observed cell shapes and the location and timing of their appearance result from a predefined program or are triggered by mechanical signals remains an open question. A challenge for the elastic framework is to address later stages of type-B inversion, the opening and closing of the phialopore, and the dynamics of type-A inversion.

We are grateful to J. Dunstan and A. Kabla for discussions at an early stage of this work, and to D. Page-Croft and C. Hitch for instrument fabrication. This work was supported in part by an Ernest Oppenheimer Early Career Research Fellowship (A. R. H. S.), the EPSRC (P. A. H.), and ERC Advanced Investigator Grant No. 247333 (S. H., P. K. T., and R. E. G.).

[1] L. Wolpert, quoted in J. M. W. Slack, *From Egg to Embryo: Determinative Events in Early Development.* (Cambridge University Press, Cambridge, England, 1986), p. 1
[2] B. He, K. Doubrovinski, O. Polyakov, and E. Wieschaus, Apical constriction drives tissue-scale hydrodynamic flow to mediate cell elongation, Nature (London) **508**, 392 (2014).
[3] L. A. Lowery and H. Sive, Strategies of vertebrate neurulation and a re-evaluation of teleost neural tube formation, Mech. Develop. **121**, 1189 (2004).
[4] M. Eiraku, N. Takata, H. Ishibashi, M. Kawada, E. Sakakura, S. Okuda, K. Sekiguchi, T. Adachi, and Y. Sasai, Self-organizing optic-cup morphogenesis in three-dimensional culture, Nature (London) **472**, 51 (2011).
[5] J. M. Sawyer, J. R. Harrell, G. Shemer, J. Sullivan-Brown, M. Roh-Johnson, and B. Goldstein, Apical constriction: A cell shape change that can drive morphogenesis, Dev. Biol. **341**, 5 (2010).
[6] D. L. Kirk, *Volvox: Molecular-Genetic Origins of Multicellularity and Cellular Differentiation* (Cambridge University Press, Cambridge, England, 1998).
[7] N. Ueki and I. Nishii, Controlled enlargement of the glycoprotein vesicle surrounding a *Volvox* embryo requires the InvB nucleotide-sugar transporter and is required for normal morphogenesis, Plant Cell **21**, 1166 (2009).
[8] K. J. Green and D. L. Kirk, Cleavage patterns, cell lineages, and development of a cytoplasmic bridge system in Volvox embryos, J. Cell Biol. **91**, 743 (1981).
[9] K. J. Green, G. L. Viamontes, and D. L. Kirk, Mechanism of formation, ultrastructure, and function of the cytoplasmic bridge system during morphogenesis in *Volvox*, J. Cell Biol. **91**, 756 (1981).
[10] G. L. Viamontes and D. L. Kirk, Cell shape changes and the mechanism of inversion in *Volvox*, J. Cell Biol. **75**, 719 (1977).
[11] D. L. Kirk and I. Nishii, *Volvox carteri* as a model for studying the genetic and cytological control of morphogenesis, Development, growth and differentiation **43**, 621 (2001).
[12] A. Hallmann, Morphogenesis in the family Volvocaceae: different tactics for turning an embryo right-side out, Protist **157**, 445 (2006).
[13] S. Höhn and A. Hallmann, There is more than one way to turn a spherical cellular monolayer inside out: Type B embryo inversion in *Volvox globator*, BMC Biol. **9**, 89 (2011).
[14] See Supplemental Material at http://link.aps.org/supplemental/10.1103/PhysRevLett.114.178101 for a movie summarizing the experimental results, supplemental methods, and additional model results.
[15] G. I. Viamontes, L. J. Fochtmann, and D. L. Kirk, Morphogenesis in *Volvox*: Analysis of critical variables, Cell **17**, 537 (1979).
[16] I. Nishii and S. Ogihara, Actomyosin contraction of the posterior hemisphere is required for inversion of the Volvox embryo, Development **126**, 2117 (1999).
[17] I. Nishii, S. Ogihara, and D. L. Kirk, A kinesin, invA, plays an essential role in *Volvox* morphogenesis, Cell **113**, 743 (2003).
[18] J. Zimmerberg and M. M. Kozlov, How proteins produce cellular membrane curvature, Nat. Rev. Mol. Cell Biol. **7**, 9 (2006); T. Kirchhausen, Bending membranes, Nat. Cell Biol. **14**, 906 (2012).
[19] J. Guven, G. Huber, and D. M. Valencia, Terasaki Spiral Ramps in the Rough Endoplasmic Reticulum, Phys. Rev. Lett. **113**, 188101 (2014).
[20] P. G. Pitrone, J. Schindelin, L. Stuyvenberg, S. Preibisch, M. Weber, K. W. Eliceiri, J. Huisken, and P. Tomancak, OpenSPIM: An open-access light-sheet microscopy platform, Nat. Methods **10**, 598 (2013).
[21] U. G. Schlösser, SAG - Sammlung von Algenkulturen at the University of Göttingen catalogue of strains 1994, Botanica acta : Berichte der Deutschen Botanischen Gesellschaft **107**, 113 (1994).
[22] D. R. Brumley, K. Y. Wan, M. Polin, and R. E. Goldstein, Flagellar synchronization through direct hydrodynamic interactions, eLife **3**, e02750 (2014).
[23] W. S. Rasband, ImageJ (US NIH, Bethesda, Maryland, 1997–2014), http://imagej.nih.gov/ij/.
[24] J. Hardin and R. Keller, The behaviour and function of bottle cells during gastrulation of Xenopus laevis, Development **103**, 211 (1988).
[25] W. Helfrich, Elastic properties of lipid bilayers: Theory and possible experiments, Z. Naturforsch. **28c**, 693 (1973).
[26] U. Seifert, Configurations of fluid membranes and vesicles, Adv. Phys. **46**, 13 (1997).
[27] A. Libai and J. G. Simmonds, *The Nonlinear Theory of Elastic Shells* (Cambridge University Press, Cambridge, England, 2006); B. Audoly and Y. Pomeau, *Elasticity and Geometry* (Oxford University Press, Oxford, England, 2010); S. Knoche and J. Kierfeld, Buckling of spherical capsules, Phys. Rev. E **84**, 046608 (2011).
[28] J. L. Kelland, Inversion in *Volvox (Chlorophyceae)*, J. Phycol. **13**, 373 (1977).
[29] R. E. Goldstein, P. B. Warren, and R. C. Ball, Shape of a Ponytail and the Statistical Physics of Hair Fiber Bundles, Phys. Rev. Lett. **108**, 078101 (2012).
[30] A. Pandey, D. E. Moulton, D. Vella, and D. P. Holmes, Dynamics of snapping beams and jumping poppers, Europhys. Lett. **105**, 24001 (2014).
[31] L. D. Landau and E. M. Lifshitz, *Theory of Elasticity*, 3rd ed. (Pergamon, Oxford, 1986).
[32] P. A. Haas and R. E. Goldstein (unpublished).